



Distinguishing the impacts of natural and anthropogenic aerosols on global gross primary productivity through diffuse fertilization effect

Hao Zhou^{1,2}, Xu Yue³, Yadong Lei⁴, Chenguang Tian^{1,2}, Jun Zhu³, Yimian Ma^{1,2}, Yang Cao^{1,2},
Xixi Yin³, and Zhiding Zhang³

¹Climate Change Research Center, Institute of Atmospheric Physics (IAP),
Chinese Academy of Sciences (CAS), Beijing 100029, China

²University of Chinese Academy of Sciences, Beijing, China

³Jiangsu Key Laboratory of Atmospheric Environment Monitoring and Pollution Control,
Jiangsu Collaborative Innovation Center of Atmospheric Environment and Equipment Technology, School of
Environmental Science and Engineering, Nanjing University of Information Science & Technology (NUIST),
Nanjing 210044, China

⁴State Key Laboratory of Severe Weather & Key Laboratory of Atmospheric Chemistry of the China
Meteorological Administration (CMA),
Chinese Academy of Meteorological Sciences, Beijing 100081, China

Correspondence: Xu Yue (yuexu@nuist.edu.cn)

Received: 19 August 2021 – Discussion started: 16 September 2021

Revised: 10 November 2021 – Accepted: 1 December 2021 – Published: 17 January 2022

Abstract. Aerosols can enhance ecosystem productivity by increasing diffuse radiation. Such diffuse fertilization effects (DFEs) vary among different aerosol compositions and sky conditions. Here, we apply a suite of chemical, radiation, and vegetation models in combination with ground- and satellite-based measurements to assess the impacts of natural and anthropogenic aerosol species on gross primary productivity (GPP) through DFE from 2001–2014. Globally, aerosols enhance GPP by 8.9 Pg C yr^{-1} under clear-sky conditions but only $0.95 \text{ Pg C yr}^{-1}$ under all-sky conditions. Anthropogenic aerosols account for 41 % of the total GPP enhancement, though they contribute only 25 % to the increment of diffuse radiation. Sulfate/nitrate aerosols from anthropogenic sources make dominant contributions of 33 % (36 %) to aerosol DFE under all-sky (clear-sky) conditions, followed by the fraction of 18 % (22 %) by organic carbon aerosols from natural sources. In contrast to other species, black carbon aerosols reduce global GPP by 0.28 (0.12) Pg C yr^{-1} under all-sky (clear-sky) conditions. Long-term simulations show that aerosol DFE increases 2.9 \% yr^{-1} under all-sky conditions mainly because of a downward trend in cloud amount. This study suggests that the impacts of aerosols and cloud should be considered in projecting future changes of ecosystem productivity under varied emission scenarios.

1 Introduction

Diffuse light enhances plant photosynthesis more efficiently than direct light (Gu et al., 2002; Alton et al., 2007; Mercado et al., 2009; Jing et al., 2010; Cirino et al., 2014; Zhou et al., 2021a, c). The cause for such a difference is that diffuse light can penetrate into the deep canopy and enhance photosynthesis of more shaded leaves with higher light use efficiency

($\text{LUE} = \text{GPP} / \text{PAR}$, gross primary productivity per photosynthetically active radiation) (Roderick et al., 2001; Gu et al., 2003; Rap et al., 2015). However, direct light is absorbed only by sunlit leaves, and much of it is wasted because these leaves are usually at the light-saturated conditions (Gu et al., 2002; He et al., 2013). As a result, increasing the diffuse radiation can help promote canopy photosynthesis through the diffuse fertilization effect (DFE).

Table 1. Summary of previous studies about aerosol DFE.

Period	Region	Method	Species	Results*	References
2000–2001	Eastern United States	Model	Aerosols	Aerosol DFE decreases NPP by 0.71 g C m^{-2} (-0.09%) in 2000 but increases NPP by 5 g C m^{-2} (0.5%) in 2001.	Matsui et al. (2008)
1960–1999	Global	Model	Cloud and aerosols	DFE enhances the land carbon sink by approximately one-quarter from 1960–1999.	Mercado et al. (2009)
2002–2003	Amazon	Flux.obs	Smoke aerosols	The increase in CO_2 uptake under high AOD is due to DFE (80%) and decreased temperature (20%).	Doughty et al. (2010)
Jul–Aug 2007	Northwest China	Flux.obs	Cloud and aerosols	Cloud dominates DFE, but aerosols lead to negative carbon uptake.	Jing et al. (2010)
2003–2010	Global	Model	Aerosols	Aerosol DFE enhances GPP by 4.9 Pg C yr^{-2} , NPP by 3.8 Pg C yr^{-2} , and NEP by 3.9 Pg C yr^{-2} .	Chen and Zhuang (2014)
1999–2009	Amazon	Flux.obs	Cloud and fire aerosols	Low AOD and cloud cover lead to relatively larger photosynthetic efficiency than high aerosol loading and thick cloud.	Cirino et al. (2014)
1998–2007	Amazon	Model	Fire aerosols	Fire aerosols enhance diffuse radiation by 3.4% – 6.8% and NPP by 1.4% – 2.8% .	Rap et al. (2015)
2003–2012	Eastern United States	Flux.obs	Aerosols	High AOD (> 0.6) enhances plant productivity for forests, but causes negative effects for croplands and grasslands.	Strada et al. (2015)
2000	Global	Model	Aerosols	Aerosol DFE increases global GPP by 1% – 2% .	Strada and Unger (2016)
1995–2013	United States	Model	Sulfate aerosols	The reductions of sulfate aerosols lead to decreased diffuse light by $0.6\% \text{ yr}^{-1}$ and GPP by $0.07\% \text{ yr}^{-1}$.	Keppel-Aleks and Washenfelder (2016)
2010	Amazon	Model	Fire aerosols	Fire aerosols increase GPP by 27% and plant respiration by 10% and decrease soil respiration by 3% .	Moreira et al. (2017)
2010–2050	Boreal North America	Model	Fire aerosols	Fire aerosols increase NPP by 8 Tg C yr^{-1} in the 2010s and 14 Tg C yr^{-1} in the 2050s due to increased diffuse radiation of 2.6 W m^{-2} (1.7%) and 4.0 W m^{-2} (2.3%).	Yue et al. (2017a)
2009–2011	China	Model	Aerosols	Aerosols increase NPP by $1.6 \pm 0.5\%$ under all-sky conditions and $35 \pm 0.9\%$ under clear-sky conditions.	Yue and Unger (2017)
2008–2017	Eurasia	Flux.obs	Aerosols	High aerosol loading increases GPP by 6% – 14% at all sites.	Ezhova et al. (2018)
2000	Global	Model	Biogenic aerosols	Biogenic aerosols enhance global NPP by $1.23 \text{ Pg C yr}^{-1}$ due to DFE.	Rap et al. (2018)
2001–2011	Global	Model	All and fire aerosols	All (fire) aerosols increase global GPP by 1.0 ± 0.2 (0.05 ± 0.3) Pg C yr^{-1} due to DFE.	Yue and Unger (2018)

Table 1. Continued.

Period	Region	Method	Species	Results*	References
2014–2015	China	Flux.obs	Aerosols	Photosynthesis of sunlit and shaded leaves increases by 0.56 % and 10.71 % due to the increase in AOD of 0.1.	Wang et al. (2018)
2000	Amazon	Model	Fire aerosols	Fire aerosols increase NPP by 5–13 Tg C yr ⁻¹ due to radiative effects.	Malavelle et al. (2019)
2018	Western North America	Flux.obs	Wildfire-smoke aerosols	Aerosols lead to GPP enhancement of 1.2 %–4.1 % compared to the previous growing season.	Hemes et al. (2020)
2006–2015	China	Model	Aerosols	Aerosols enhance GPP by 0.36 Pg C yr ⁻¹ (5 %), and DFE makes the dominant contribution (59 %–62 %).	Xie et al. (2020)

* Carbon metrics include net primary productivity (NPP), net ecosystem productivity (NEP), and gross primary productivity (GPP)

Atmospheric aerosols can alter the quality of sunlight reaching Earth's surface by absorbing and scattering solar insolation (Zhou et al., 2021b). The aerosol-induced radiative impacts on terrestrial ecosystem productivity have been investigated in both observational and modeling studies (Table 1). Observations found unexpected decline of atmospheric carbon dioxide in 1990s, which was attributed to the increase in vegetation carbon uptake owing to the massive eruption of Mt. Pinatubo in 1991 (Roderick et al., 2001). Sulfate aerosols from volcanic eruption almost doubled diffuse radiation in the clear sky, leading to the enhancement of plant productivity by 23 % at Harvard forests in 1992 (Gu et al., 2003). With the development of ground-based instruments and satellite remote sensing, more observational data have been applied to detect the aerosol DFE. Strada et al. (2015) estimated aerosol DFE on plant productivity using aerosol optical depth (AOD) from satellite cloudless observations at 10 flux sites, and they found that aerosols enhance GPP by 13 % in midday hours under high-AOD conditions (> 0.4) for deciduous and mixed forests. Similarly, Ezhova et al. (2018) found that aerosols increase clear-day diffuse fraction from 0.11 to 0.27 at five remote sites in Eurasia, leading to the enhancement of site-level GPP by 6 %–14 %.

In contrast to the large benefits on clear days, the aerosol DFE is limited on cloudy days. Kanniah et al. (2013) explored cloud direct radiative effects on canopy productivity using observed carbon fluxes and radiation in tropical savannas, and they found that thick cloud masked aerosol DFE and reduced GPP by 26 %. Cirino et al. (2014) also found that aerosol DFE cannot increase plant photosynthesis under cloudy conditions. These studies indicated that aerosol DFE is subject to sky conditions and aerosol loading because the potential benefits from DFE can be offset or even reversed by simultaneous reductions in direct radiation caused by thick cloud or high aerosol loading (Alton, 2008; Cirino et al., 2014; Yue and Unger, 2017; Zhou et al., 2021b).

Although observational studies directly estimate site-level aerosol DFE, they are not able to reveal regional or global aerosol DFE due to the limited spatiotemporal coverage. On the global scale, studies using varied models showed that aerosol DFE enhances global GPP by 4.9 Pg C yr⁻¹ (Chen and Zhuang, 2014), 1 %–2 % (Strada and Unger, 2016), and 1.0 ± 0.2 Pg C yr⁻¹ (Yue and Unger, 2018) in different periods. Rap et al. (2018) specifically explored DFE from biogenic aerosols and found that biogenic aerosols enhance global net primary productivity (NPP) by 1.23 Pg C yr⁻¹. Regionally, Matsui et al. (2008) applied a land surface model and estimated that aerosol DFE decreased NPP by 0.09 % in 2000 but increased NPP by 0.5 % in 2001 over the eastern US, because the cloud optical depth was about half in 2001 relative to 2000. At the same region, Keppel-Aleks and Washenfelder (2016) estimated sulfate aerosol DFE using the Community Earth System Model and found that the reductions of sulfate aerosols by 3.0 ± 0.6 % yr⁻¹ led to reductions of 0.6 % yr⁻¹ in diffuse radiation and 0.07 % yr⁻¹ in regional GPP from 1995–2013. In Amazon, fire aerosols are estimated to play a role in varied DFEs among different studies (Rap et al., 2015; Moreira et al., 2017; Yue and Unger, 2018; Malavelle et al., 2019). For example, Rap et al. (2015) found that fire aerosols enhance NPP by 1.4 %–2.8 % while Moreira et al. (2017) estimated that fire aerosols enhance GPP by 27 %. Such differences are mainly attributed to the high aerosol loading in Moreira et al. (2017) for September 2010 but much lower loading in Rap et al. (2015) for the 10-year (1998–2007) averages. Although these studies assessed the DFE of total aerosols or the specific species (e.g., sulfate, fire, or biogenic), the individual DFEs of natural and anthropogenic aerosols on global terrestrial productivity remain unclear.

In this study, we explore the impacts of natural and anthropogenic aerosol DFE on global GPP from 2001–2014 using both multi-source observations and a series of well-validated

models. A chemical transport model (CTM) is used to predict changes of natural and anthropogenic aerosol concentrations. A radiative transfer model is applied to calculate the perturbations in direct and diffuse PAR caused by aerosols. A global dynamic vegetation model is used to quantify changes of global GPP caused by aerosol DFE. The main objectives are (1) to distinguish the DFEs of natural and anthropogenic aerosols on global GPP and (2) to explore the different characteristics of aerosol DFEs for varied species.

2 Methods

2.1 Chemical transport model

The Goddard Earth Observing System coupled with Chemistry (GEOS-Chem, <http://geos-chem.org>, last access: 15 June 2021) is a three-dimensional (3-D) CTM for simulating atmospheric compositions and air quality (Bey et al., 2001). Global anthropogenic emissions from 2001–2014 are from the Community Emissions Data System (CEDS) inventory (<http://www.globalchange.umd.edu/ceds/>, last access: 15 June 2021). The CEDS inventory has been used as anthropogenic emissions in the Coupled Model Intercomparison Project Phase 6 (CMIP6), and this emission database relies on existing energy consumption datasets and regional or country-specific inventories to produce trends over recent decades (Hoesly et al., 2018). The specific emission species include aerosols (black carbon, organic carbon), aerosol precursors, and reactive compounds (SO_2 , NO_x , NH_3 , CH_4 , CO , and non-methane volatile organic compounds (VOCs)) (Supplement Table S1). To estimate modeling uncertainties due to emission inventories, the Emissions Database for Global Atmospheric Research (EDGAR) inventory vision 4.3.1 (<https://edgar.jrc.ec.europa.eu/>, last access: 15 June 2021) from 2001–2010 is also used as alternative anthropogenic emissions for the GEOS-Chem model. For natural emissions, the Global Fire Emission Database (GFED) version 4 inventory is used to represent emissions from open fires (<http://www.globalfiredata.org/>, last access: 15 June 2021). Biogenic VOC emissions are calculated using the Model of Emissions of Gases and Aerosols from Nature (MEGAN v2.1) (Guenther et al., 2012). Natural emissions of sea salt (Jaeglé et al., 2011), dimethyl sulfate (Breider et al., 2017), volcanic SO_2 (Fisher et al., 2011), and NH_3 are from the Global Emissions Initiative (GEIA, <http://www.geiacenter.org/>, last access: 15 June 2021). In this study, GEOS-Chem version 12.0.0 is used to simulate concentrations of natural and anthropogenic aerosols at a horizontal resolution of $4^\circ \times 5^\circ$ and 47 vertical layers. The CTM is driven with assimilated meteorology from the Modern-Era Retrospective analysis for Research and Applications, version 2 (MERRA2).

2.2 Radiative transfer model

The Column Radiation Model (CRM) is the standalone version of the radiative transfer module used by the NCAR Community Climate Model (<http://www.cesm.ucar.edu/models/>, last access: 12 July 2021). In this model, aerosol direct radiative effects including absorbing and scattering processes are calculated at 20 vertical layers from the surface to 0.5 hPa at hourly intervals (Yue and Unger, 2017). The CRM utilizes aerosol profiles of all species simulated by GEOS-Chem, including sulfate, nitrate, black carbon (BC), organic carbon (OC), dust (clay and silt), and sea salt (coarse and accumulation modes). Aerosol optical parameters (e.g. single-scattering albedo, extinction coefficients, and asymmetric parameters) are adopted from Yue and Liao (2012) for sea salt, Yue et al. (2010) for mineral dust, and the RegCM4 model for other species (Giorgi et al., 2012). In this study, the CRM is used to simulate aerosol-induced perturbations in surface radiative fluxes including diffuse and direct PAR. The model is driven with hourly $1^\circ \times 1^\circ$ meteorology from MERRA-2 reanalyses and 3-hourly cloud cover and liquid water path from CERES SYN1deg (<http://ceres.larc.nasa.gov>, last access: 12 July 2021).

2.3 Dynamic vegetation model

The Yale Interactive terrestrial Biosphere (YIBs) model is a process-based vegetation model that dynamically simulates tree growth and leaf area changes (Yue and Unger, 2015). The model uses the well-established leaf photosynthesis (Farquhar et al., 1980) and stomatal conductance schemes (Ball et al., 1987). The canopy is divided into sunlit and shaded portions to separate photosynthetic responses to diffuse and direct light (Spitters et al., 1986). We distinguish light absorption between sunlit (receiving both diffuse and direct light) and shaded leaves (receiving only diffuse light), and we derive canopy photosynthesis as the sum of that from sunlit and shaded leaves:

$$A_{\text{total}} = A_{\text{sunlit}} \times F_{\text{sunlit}} + A_{\text{shaded}} \times (1 - F_{\text{sunlit}}), \quad (1)$$

where A_{sunlit} and A_{shaded} are the photosynthesis of sunlit and shaded leaves, respectively. The fraction of sunlit leaf area F_{sunlit} is calculated as

$$F_{\text{sunlit}} = e^{-kL}. \quad (2)$$

Here, L is leaf area index (LAI) at one canopy layer, and k is extinction coefficient defined as $0.5/\cos\alpha$ (solar zenith α). Compared with global in situ measurements, this canopy radiative transfer scheme reasonably captures the different responses of GPP to direct and diffuse radiation (Yue and Unger, 2018; Zhou et al., 2021a). For this study, we use the original scheme without modifications.

Simulated GPP by the YIBs model has been validated using ground-based observations at 145 sites and yielded an

average correlation coefficient of 0.76 for all sites (Yue and Unger, 2015). The simulated global GPP also shows reasonable spatiotemporal variations compared with satellite retrievals (Yue et al., 2015). Recently, the model joined the multi-model ensemble project of TRENDY to provide the estimates of global carbon budget (Friedlingstein et al., 2020). In this study, the YIBs model is used to isolate impacts of aerosol-induced PAR changes on GPP on the global scale. The model is driven with $1^\circ \times 1^\circ$ meteorological forcing from MERRA-2 reanalyses and PAR (both diffuse and direct) simulated by CRM. Land cover product from MODIS is used as vegetation coverage for the YIBs model (Yue et al., 2021), and observed CO₂ concentrations from Mauna Loa are also used (Yue et al., 2015).

2.4 Model simulations

We perform two GEOS-Chem runs, as well as 22 CRM and YIBs runs, to isolate aerosol direct radiative impacts on GPP at different sky conditions (Table S2 in the Supplement). The GEOS-Chem runs GC_ALL and GC_NAT are driven with the same meteorology and emissions except that the former includes all sources of emissions while the latter excludes only anthropogenic emissions. Following the methods in Nascimento et al. (2021) and Ryu et al. (2013), we use the differences between GC_ALL and GC_NAT to represent aerosol concentrations contributed by anthropogenic sources. In this practice, the sums of natural and anthropogenic aerosol concentrations are equal to the total aerosol concentrations without non-linear effects. Both GC_ALL and GC_NAT runs provide 3-D concentrations of different aerosol types including sulfate, nitrate, OC, BC, dust, and sea salt. The CRM runs aim to calculate aerosol-induced PAR changes using aerosol profiles simulated by GEOS-Chem. These runs can be divided into two groups, with CLD runs (all-sky conditions) are forced with observed cloud profiles while CLR runs (clear-sky conditions) forced without any cloud coverage. CRM_ALL and CRM_NAT are driven with aerosol profiles of all species from GC_ALL and GC_NAT, respectively. The impacts of individual aerosol species on PAR are isolated with individual aerosol profiles from either GC_ALL or GC_NAT. For example, OC from GC_ALL and cloud amounts from CERES SYN1deg are used to drive CRM (CRM_ALL_OCCLD) so as to isolate the impacts of OC aerosols on PAR under all-sky conditions. It should be noted that such a setup cannot resolve the interactive responses among aerosol species, because the sum of individual aerosol effects is not necessarily equal to the net impact of all aerosols. The magnitude of these non-linear effects will be evaluated accordingly. For each of CRM runs, the predicted diffuse and direct PAR values are used as input for the YIBs model to simulate GPP changes caused by aerosol DFEs. For YIBs runs, other forcings (e.g., CO₂ concentrations and climate meteorology) except diffuse and direct PAR are kept

the same in all runs, so as to exclude their impacts on global GPP.

2.5 Observations for model evaluations

We use site-level measurements of carbon fluxes from the FLUXNET2015 product (<http://fluxnet.fluxdata.org/>, last access: 15 August 2020) to validate model GPP and its responses to diffuse and direct radiation. We select 10 sites providing simultaneous observations of diffuse radiation and GPP at half-hourly time intervals for at least 8 years. On the global scale, observed AOD is retrieved from the Moderate Resolution Imaging Spectroradiometer (MODIS, <https://modis.gsfc.nasa.gov>, last access: 14 August 2020), and GPP is derived using the global OCO-2-based SIF product (Li and Xiao, 2019). The all-sky and clear-sky shortwave radiation are adopted from CERES SYN1deg (<http://ceres.larc.nasa.gov>, last access: 12 July 2021) to validate the CRM radiative transfer model. To evaluate the performance of models, we use statistical metrics including correlation coefficients (R) and normalized mean biases (NMB) defined as follows:

$$R = \frac{\sum_{i=1}^{i=n} (M_i - \bar{M})(O_i - \bar{O})}{\sqrt{\sum_{i=1}^{i=n} (M_i - \bar{M})^2 \times \sum_{i=1}^{i=n} (O_i - \bar{O})^2}}, \quad (3)$$

$$\text{NMB} = \frac{\sum_{i=1}^{i=n} (M_i - O_i)}{\sum_{i=1}^{i=n} O_i}, \quad (4)$$

where O_i and M_i are observed and modeled values, respectively. \bar{O} and \bar{M} are the averages of the observed and modeled values. In this study, R and NMB are used to evaluate the performance of models on the spatial scale, and the Student t test is used to examine the significance of correlation coefficients and long-term trends.

3 Results

3.1 Model evaluations

The YIBs model simulates a reasonable spatial pattern of GPP compared to observations (Fig. S1) with a high correlation coefficient (R) of 0.88 ($p < 0.01$) and a low normalized mean bias (NMB) of -2.3% . Similarly, modeled AOD from the GEOS-Chem model reproduces the observed spatial pattern from the MODIS product with a high R of 0.78 ($p < 0.01$), though it overestimates the mean AOD by 21.7% in eastern China and 37.9% in southern Africa while it underestimates AOD by 35.7% in Amazon, 25.2% in central Africa, and 53.4% in southeast Asia, leading to a global NMB of -25.8% .

CRM driven with aerosol concentrations from GEOS-Chem shows similar patterns of shortwave radiation to the satellite observations (Fig. S2). The simulations match observations well, with a high R of 0.98 and low NMB of 4.1% under all-sky conditions, and they show even better perfor-

mance with R of 1 and NMB of 3.7 % under clear-sky conditions. Although CRM presents high R and low NMB under both sky conditions, evaluations still show that modeled shortwave radiation is higher than observations. Such overestimation may be related to the underestimation of simulated AOD (Fig. S1), which leads to more shortwave radiation reaching the surface. We further evaluate the simulated diffuse fraction (DF) with satellite observations (Fig. S3). Simulations reproduce the observed spatial pattern with high R of 0.82 and low NMB of -0.1 % on the global scale, but they overestimate regional DF over high latitudes and underestimate DF over Asia. Moreover, CRM simulates reasonable aerosol direct radiative effects compared to multiple radiative transfer models as shown in Yue and Unger (2018).

We then compared the simulated and observed GPP responses to direct (diffuse fraction < 0.2) and diffuse radiation (diffuse fraction > 0.8) (Fig. 1). Observations and simulations show that diffuse light can increase GPP more efficiently than direct radiation as shown by the higher GPP–PAR slopes at diffuse conditions. Similar results were achieved by Mercado et al. (2009) and Yue and Unger (2018) using the same methods. The diffuse fertilization efficiency, percentage changes in GPP per unit diffuse PAR, is estimated to be $0.45 \text{ \% W}^{-1} \text{ m}^2$ – $0.7 \text{ \% W}^{-1} \text{ m}^2$ for observations and $0.3 \text{ \% W}^{-1} \text{ m}^2$ – $0.69 \text{ \% W}^{-1} \text{ m}^2$ for simulations. As a result, the YIBs model can reasonably reproduce varied light-response curves so as to isolate GPP responses to direct and diffuse radiation.

3.2 Changes of PAR by aerosols

Aerosols reduce total PAR but enhance diffuse PAR at the surface. Relative to PAR changes without aerosols, appearance of aerosols on average reduces total surface PAR by 1.52 W m^{-2} under all-sky conditions and 2.73 W m^{-2} under clear-sky conditions on the global scale. Under all-sky conditions, aerosols enhance diffuse PAR by 1.26 W m^{-2} (Fig. 2a) but reduce direct PAR by 2.78 W m^{-2} (Fig. S4a). These changes are larger in clear-sky conditions, with enhancement of diffuse PAR by 4.98 W m^{-2} (Fig. 2d) and reduction of direct PAR by 7.71 W m^{-2} (Fig. S4d). Regionally, aerosols cause large enhancement of diffuse PAR ($> 3 \text{ W m}^{-2}$) over southern US, Australia, Europe, and northern Asia under clear-sky conditions (Fig. 2d). However, these enhancements of diffuse PAR are largely dampened under all-sky conditions (Fig. 2a). Similar changes in diffuse radiation by aerosols are predicted by Chen and Zhuang (2014) and Rap et al. (2018), though the former study yielded much larger changes in radiation, and the latter examined only biogenic aerosols. The cause of smaller PAR changes under all-sky conditions is that cloud tends to weaken aerosol radiative forcing by amplifying absorption and diminishing scattering (Paulot et al., 2018).

Relative to diffuse PAR changes without aerosols, natural aerosols dominate aerosol-induced PAR changes by en-

hancing diffuse PAR of 0.93 W m^{-2} (Fig. 2b) and reducing direct PAR of 2.05 W m^{-2} (Fig. S4b) under all-sky conditions. As a comparison, anthropogenic aerosols induce much smaller changes of diffuse radiation by 0.33 W m^{-2} and direct radiation of -0.72 W m^{-2} (Figs. 2c and S4c). Natural aerosols mainly influence PAR fluxes in northern Africa owing to a large amount of dust aerosols, while anthropogenic aerosols dominate PAR changes in eastern China, India, and the eastern US due to the large anthropogenic emissions. Under clear-sky conditions, natural aerosols enhance diffuse PAR by 3.79 W m^{-2} (Fig. 2e) and reduce direct PAR by 5.84 W m^{-2} (Fig. S4e), and anthropogenic aerosols on average enhance diffuse PAR by 1.19 W m^{-2} and reduce direct PAR by 1.88 W m^{-2} .

We further explore the contributions of individual aerosol species to the changes of diffuse and direct PAR under all-sky conditions (Figs. S5 and S6). On the global scale, sulfate and nitrate aerosols enhance diffuse PAR by 0.57 W m^{-2} , accounting for 51 % of aerosol-induced diffuse PAR changes. Meanwhile, diffuse PAR is enhanced 0.05, 0.37, and 0.25 W m^{-2} by the scattering effects of OC, dust, and sea salt aerosols. However, BC aerosols reduce diffuse PAR by 0.06 W m^{-2} due to the strong absorption. The changes of direct PAR caused by all aerosol species are negative, especially that by sulfate and nitrate (-0.97 W m^{-2}), dust (-0.86 W m^{-2}), and sea salt (-0.5 W m^{-2}). Generally, natural aerosols dominate changes of diffuse and direct PAR owing to the large contributions from dust and sea salt aerosols. However, sulfate, nitrate, and BC aerosols from anthropogenic sources dominate the changes of diffuse and direct PAR over eastern China, India, and the eastern US.

3.3 DFE by natural and anthropogenic aerosols

We quantify the percentage changes of global GPP caused by aerosol DFE. Relative to GPP changes without aerosols, aerosol DFE enhances global GPP by 0.65 % ($0.95 \pm 0.13 \text{ Pg C yr}^{-1}$) under all-sky conditions (Fig. 3a). Relatively high enhancements (> 2 %) in GPP are found over middle latitudes (20 – 50° N) following the changes of diffuse PAR (Fig. 2a). The DFE of natural aerosols enhances global GPP by 0.38 % ($0.56 \pm 0.1 \text{ Pg C yr}^{-1}$), mainly over the Middle East and northern Africa due to dust aerosols (Figs. 4a and 5g). The DFE of anthropogenic aerosols enhances global GPP up to 0.27 % ($0.39 \pm 0.04 \text{ Pg C yr}^{-1}$), especially over populous regions including northeast China, the Middle East, and the contiguous US (Fig. 4b).

Under clear-sky conditions, aerosol DFE enhances global GPP up to 7.8 % ($8.91 \pm 0.26 \text{ Pg C yr}^{-1}$) (Fig. 3c), which is around 9.5 times that under all-sky conditions (Fig. 3a). In most regions, aerosol DFE increases GPP by more than 4 %, with the maximum enhancement of 22.7 % in East Asia. The DFE of natural aerosols enhances global GPP by 4.6 %, with large changes over the Amazon, central Africa, boreal Asia, and North America (Fig. 4c). Meanwhile, anthro-

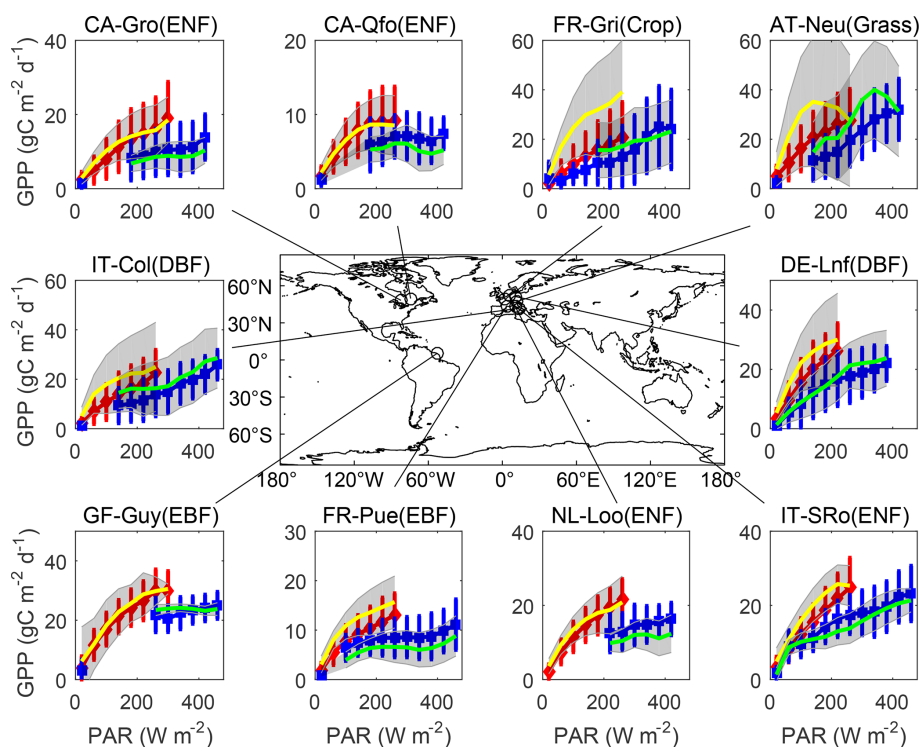


Figure 1. Simulated and observed GPP responses to direct and diffuse radiation. The comparisons are performed at 10 FLUXNET sites where more than 8 years of observations are available. For each site, hourly observations are divided into direct and diffuse conditions if diffuse fraction is < 0.2 (blue squares) and > 0.8 (red diamonds), respectively. The classified observations are averaged over PAR bins of 40 W m^{-2} , with error bars indicating 1 standard deviation of GPP for each bin. Similarly, simulations are also divided into direct (green) and diffuse (yellow) bins of PAR, with gray shading indicating 1 standard deviation. The plant function types include evergreen broadleaf forest (EBF), evergreen needleleaf forest (ENF), deciduous broadleaf forest (DBF), grassland (Grass), and cropland (Crop). The site name and vegetation type are listed on the title of each panel.

pogenic aerosols enhance global GPP by 3.2 %, mainly located in the eastern US, Europe, boreal Asia, India, and East Asia (Fig. 4d).

We further quantify the contributions of anthropogenic aerosols to the total aerosol DFE. Although cloud masks aerosol DFE and significantly reduces GPP enhancement, the contributions of anthropogenic aerosols remain similar between all-sky (Fig. 3b) and clear-sky (Fig. 3d) conditions. Relatively high contributions ($> 50\%$) are located at low latitudes to mid-latitudes including North America, Europe, and eastern China. Low contributions ($< 50\%$) are found at other regions such as Africa, South America, and Australia. On the global scale, anthropogenic aerosols on average contribute to 41 % of the total aerosol DFE under all-sky conditions (Fig. 4a and b). Anthropogenic aerosols dominate DFE over 30.5 % of land grids under all-sky conditions, but only 19.5 % under clear-sky conditions (Fig. 3b and d). The most significant differences are located boreal Europe where the anthropogenic aerosols make dominant contributions to DFE under clear-sky conditions while the natural species dominate under all-sky conditions.

3.4 DFE by individual aerosol species

We isolate the DFE of individual aerosol species on global GPP (Figs. 5 and S7), and we found that sulfate and nitrate aerosols dominate the aerosol DFE on the global scale. Under all-sky conditions, sulfate and nitrate aerosols average enhance GPP by $0.79 \text{ Pg C yr}^{-1}$, to which anthropogenic sources contribute $0.58 \text{ Pg C yr}^{-1}$ (Fig. 5f). OC aerosols increase global GPP by $0.47 \text{ Pg C yr}^{-1}$, to which natural sources contribute $0.32 \text{ Pg C yr}^{-1}$ (Fig. 5c). As the dominant natural species, dust and sea salt are generated from non-vegetated areas. They can increase GPP of downwind land regions by $0.17 \text{ Pg C yr}^{-1}$ (Fig. 5g) and $0.06 \text{ Pg C yr}^{-1}$ (Fig. 5h), respectively. Different from the above species, BC aerosols lead to negative impacts on GPP up to $-0.28 \text{ Pg C yr}^{-1}$ globally due to the strongly absorbing radiative effects. Regionally, such negative effects are prominent over central Africa from biomass burning (Fig. 5a) and eastern China from anthropogenic emissions (Fig. 5b).

Under clear-sky conditions, scattering aerosols show larger DFE compared to the all-sky conditions. Relative to GPP changes without aerosols, sulfate and nitrate aerosols increase global GPP by $5.18 \text{ Pg C yr}^{-1}$, which is 6.6 times

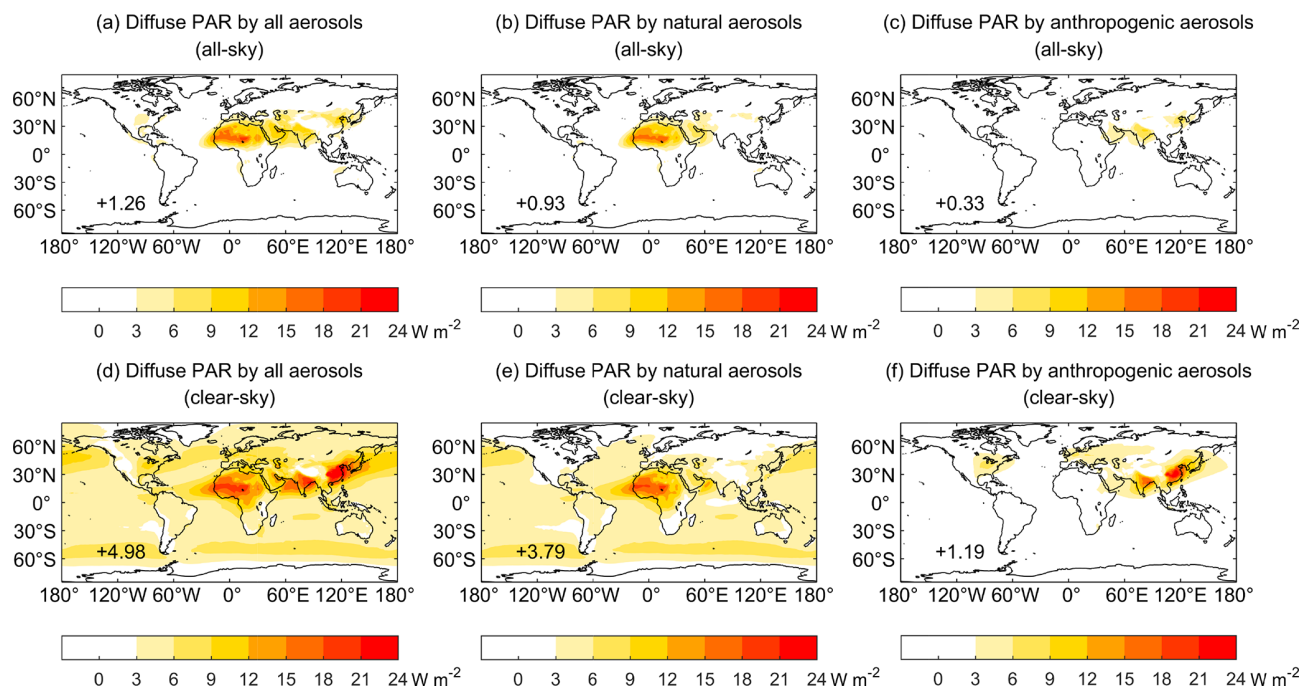


Figure 2. Global annual changes of diffuse PAR at the surface by all, natural, and anthropogenic aerosols under all-sky conditions (a–c) and clear skies (d–f). The aerosol species include natural (BC, OC, dust, sea salt, sulfate, and nitrate) and anthropogenic (BC, OC, sulfate, and nitrate) aerosols. The total changes in PAR caused by different aerosol sources are shown on corresponding panels. Changes of diffuse PAR caused by individual aerosol species are shown in Fig. S4. The units are $W m^{-2}$.

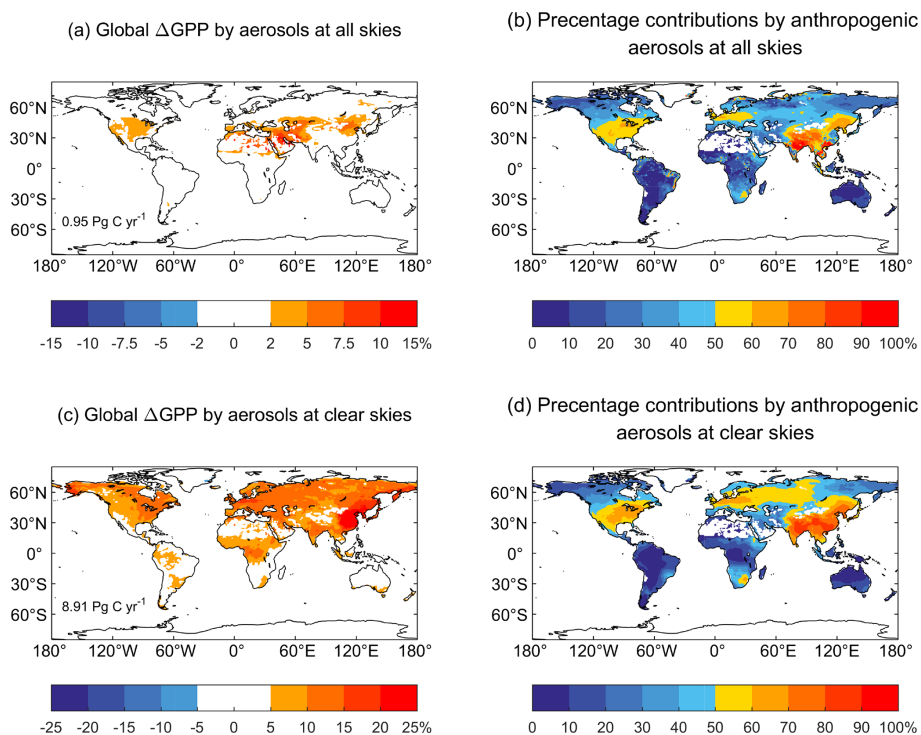


Figure 3. Percentage changes in annual GPP caused by the aerosol diffuse fertilization effect and percentage contributions by anthropogenic aerosols at (a, b) all skies and (c, d) clear skies. The DFE of all aerosols (natural + anthropogenic) are shown on the left, and the contributions by anthropogenic aerosols alone are shown on the right.

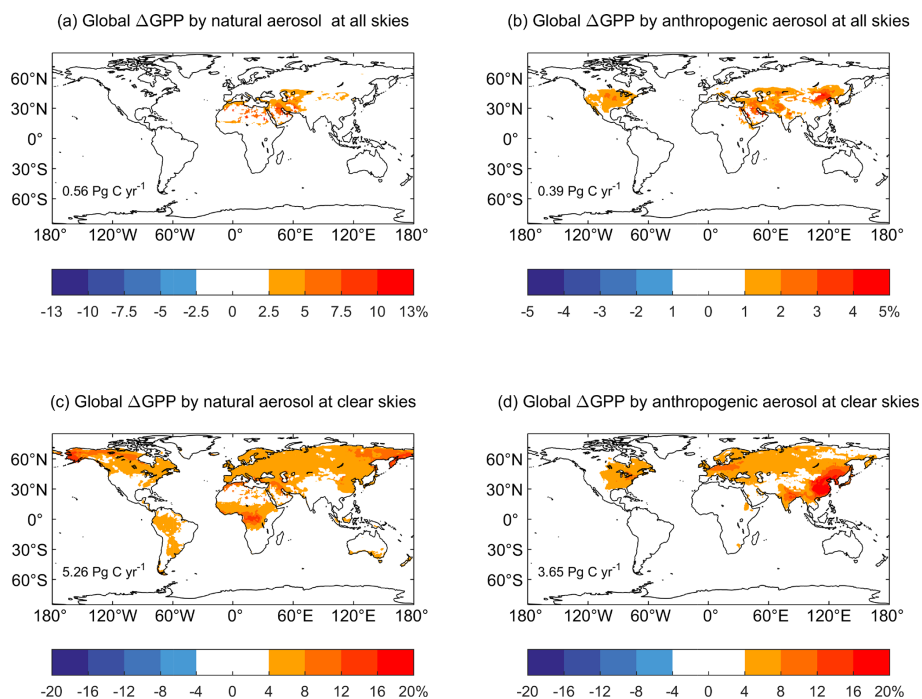


Figure 4. Percentage changes in annual GPP by (a, c) natural and (b, d) anthropogenic aerosols under (a, b) all-sky and (c, d) clear-sky conditions. The total changes in GPP caused by different aerosol sources are shown in corresponding panels. Please notice that the color scales for natural and anthropogenic aerosols are different. The units are percent.

that under all-sky conditions. The DFE of OC aerosols also largely increases to $2.89 \text{ Pg C yr}^{-1}$, in which $2.21 \text{ Pg C yr}^{-1}$ is from natural sources. Dust and sea salt aerosols lead to positive impacts on global GPP by 1.32 and $0.48 \text{ Pg C yr}^{-1}$, respectively. In contrast, BC aerosols reduce global GPP by $0.12 \text{ Pg C yr}^{-1}$, much weaker than the magnitude of $0.28 \text{ Pg C yr}^{-1}$ under all-sky conditions. Such a change mainly follows the larger diffuse absorption by BC aerosols under all-sky conditions (0.06 W m^{-2}) than that under clear-sky conditions (0.02 W m^{-2}).

We then identify the aerosol species making the dominant contributions to the total aerosol DFE (Fig. 6). Under all-sky conditions, sulfate and nitrate aerosols lead the DFE at 65 % of the grid cells (Fig. 6a) and account for 44.7 % of the total absolute GPP changes (Fig. 6c). The secondary contribution is from OC aerosols, which account for 26.7 % of the total DFE. Dust and sea salt aerosols contribute to the total DFE by 9.5 % and 3.4 %, respectively (Fig. 6c). BC aerosols exert negative DFE, the absolute value of which is equivalent to 15.8 % of the total DFE. Regionally, sulfate and nitrate aerosols lead DFE in eastern China, India, the eastern US, and Europe, while dust aerosols dominate DFE in the Middle East (Fig. 6e and f). Under clear-sky conditions, the percentage contributions of sulfate and nitrate aerosols to the total DFE further increase to 51.8 % on the global scale (Fig. 6d). OC, dust, and sea salt aerosols show comparable contributions to DFE as those under all-sky conditions. How-

ever, the absolute ratios by BC aerosols significantly reduce to 1.2 %, because BC-induced DFE is limited while DFE of other species is significantly strengthened under clear-sky conditions (Fig. S7).

We further explore the interannual variations in GPP changes caused by aerosol DFE from natural and anthropogenic sources (Fig. 7). Under all-sky conditions, aerosol DFE significantly ($p < 0.05$) increases by $2.89 \% \text{ yr}^{-1}$ ($24.6 \text{ Tg C yr}^{-2}$) on the global scale (Fig. S8a). Such enhancement is mainly located in northeastern China, India, central Africa, and Europe (Fig. S9a). Natural aerosols lead to a positive trend of $4.7 \% \text{ yr}^{-1}$ in the global GPP (22 Tg C yr^{-2}), which is 6 times of the trend of $0.67 \% \text{ yr}^{-1}$ (2.6 Tg C yr^{-2}) from anthropogenic aerosols (Fig. 7a). Under clear-sky conditions, aerosol DFE increases by only $0.4 \% \text{ yr}^{-1}$ (Fig. S8b), much lower than that under all-sky conditions (Fig. S8a). Both the DFE trends from natural and anthropogenic aerosols are limited (Fig. 7b). The contrast of DFE trends between different sky conditions is related to the changes of cloud amount, which shows a significant reduction trend of $0.38 \% \text{ yr}^{-1}$ in 2001–2014 (Fig. S8c), especially over the Amazon and eastern US (Fig. S9d). The reduction of cloud helps increase or maintain aerosol DFE under all-sky conditions (Fig. S9c). The trend of all-sky aerosol DFE is mainly contributed by dust aerosols from natural sources, which increases by $4.75 \% \text{ yr}^{-1}$ from 2001–2014 (Fig. 7c). The trend of clear-sky aerosol DFE is mainly attributed to

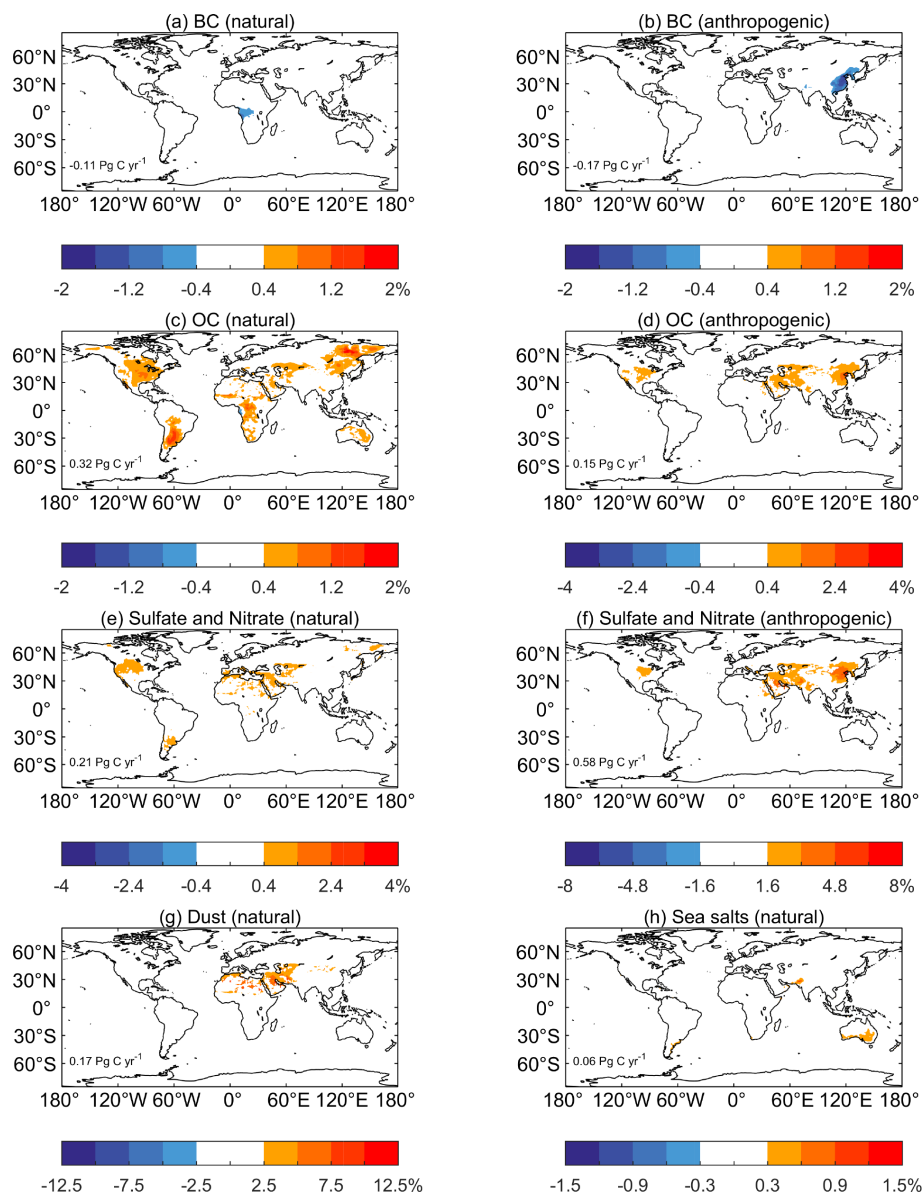


Figure 5. Percentage changes in annual GPP by specific natural and anthropogenic aerosols under all-sky conditions. The global changes in GPP caused by individual aerosol species (BC, OC, sulfate and nitrate, dust and sea salt aerosols) from different sources (natural and anthropogenic) are shown in corresponding panels. Please notice that the color scales for different aerosol species are different. The units are percent.

sulfate and nitrate aerosols, which increase by $0.44\% \text{ yr}^{-1}$ from 2001–2014 (Fig. 7d).

The differences between natural and anthropogenic aerosol DFE are inconsistent at varied sky conditions (Fig. 7). For the year 2003, ΔGPP by natural aerosols is very close to that by anthropogenic aerosols under all-sky conditions (Fig. 7a). However, the same year sees large differences of ΔGPP between different sources of aerosols in clear-sky conditions (Fig. 7b). Analyses show that increased cloud amount weakens aerosol DFE, especially over central Africa and boreal Asia, with high loading of natural aerosols

before 2003 (Fig. S11a), but decreased cloud amount enhances natural aerosol DFE over the Amazon, central Africa, and boreal Asia after 2003 (Fig. S11b). These opposite trends of cloud over regions with a high loading of natural aerosols lead to a turning point for natural aerosol DFE in 2003 under all-sky conditions.

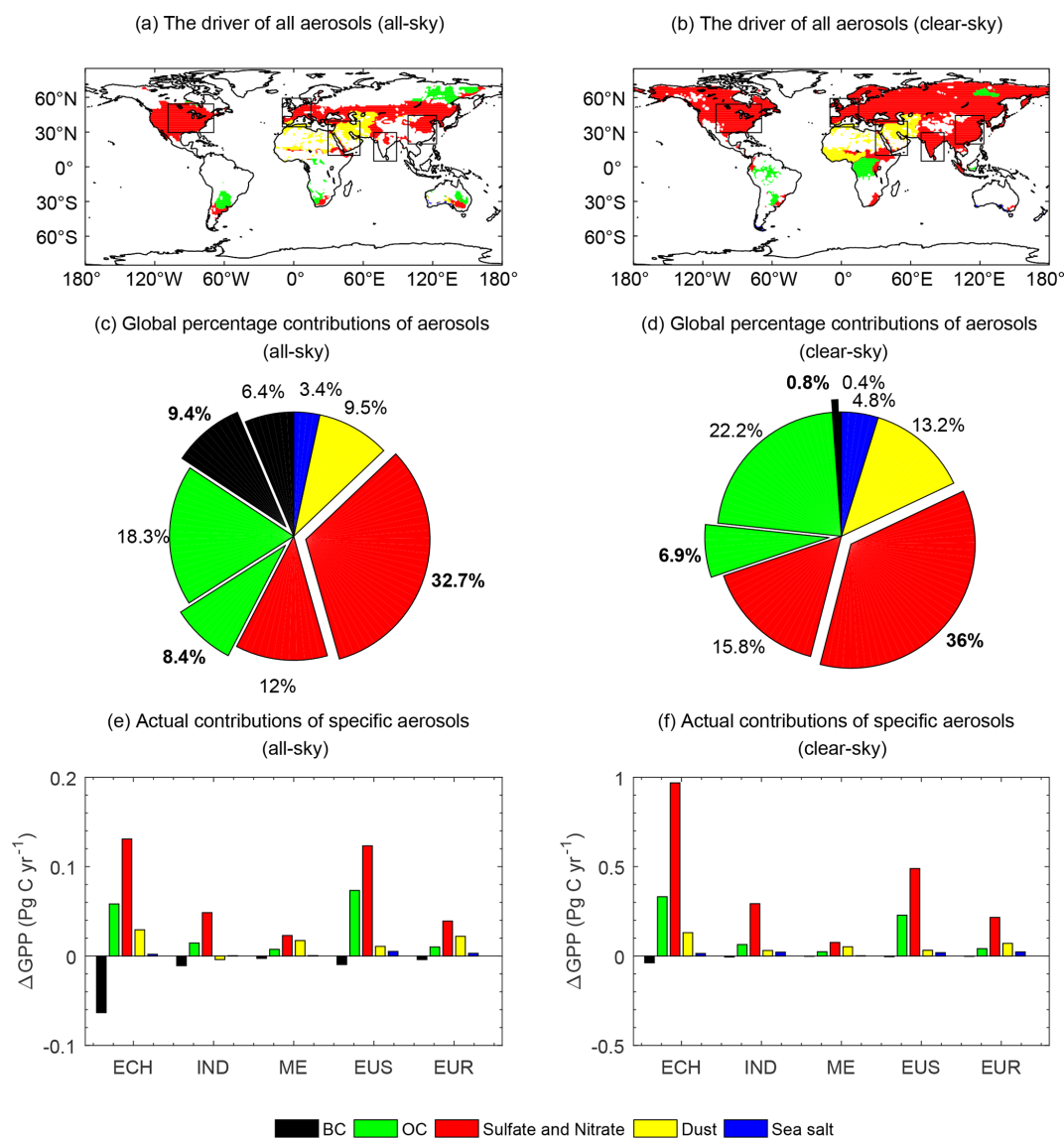


Figure 6. (a, b) Dominant aerosol species contributing to the simulated changes in annual GPP, (c, d) percentage contributions of aerosol species to global GPP, and (e, f) actual DFE of aerosol species in specific regions under (a, c, e) all skies and (b, d, f) clear skies. The contributions in (c) and (d) are calculated as the ratios of absolute DFE, as BC aerosols induce negative DFE. The normal (bold) fonts in (c) and (d) represent aerosol species from natural (anthropogenic) sources. Regions with relatively high percentage changes in GPP ($> 1\%$ for all-sky and $> 5\%$ for clear sky) by aerosols are shown in (a) and (b). The regions include eastern China (ECH), India (INA), the Middle East (ME), the eastern US (EUS), and Europe (EUR), which are marked as black boxes in (a) and (b). Black, green, red, yellow, and blue represent the effects of BC, OC, sulfate and nitrate, dust, and sea salt aerosols, respectively.

4 Discussion

4.1 Factors influencing aerosol DFE

We quantified the impacts of sky conditions, emission sources, and aerosol species on terrestrial ecosystem productivity through aerosol DFE. In our simulations, aerosols increase global GPP by $8.91 \text{ Pg C yr}^{-1}$ under clear-sky conditions but only $0.95 \text{ Pg C yr}^{-1}$ under all-sky conditions. Similarly, Cohan et al. (2002) and Yue and Unger (2017) found

aerosol DFE was limited under cloudy skies. Cloud can mask aerosol DFE by modifying both the quantity and quality of aerosol radiative perturbations (Yu et al., 2006). First, cloud weakens the impacts of aerosols on both direct and diffuse radiation (Figs. 2 and S4) by reducing the total sunlight available for the extinction by aerosols (Kinne, 2019). Therefore, the smaller changes in diffuse PAR by aerosols under all-sky conditions (Fig. 2) result in lower DFE than those under clear-sky conditions. Second, cloud significantly reduces direct radiation and limits the potential of increasing GPP by

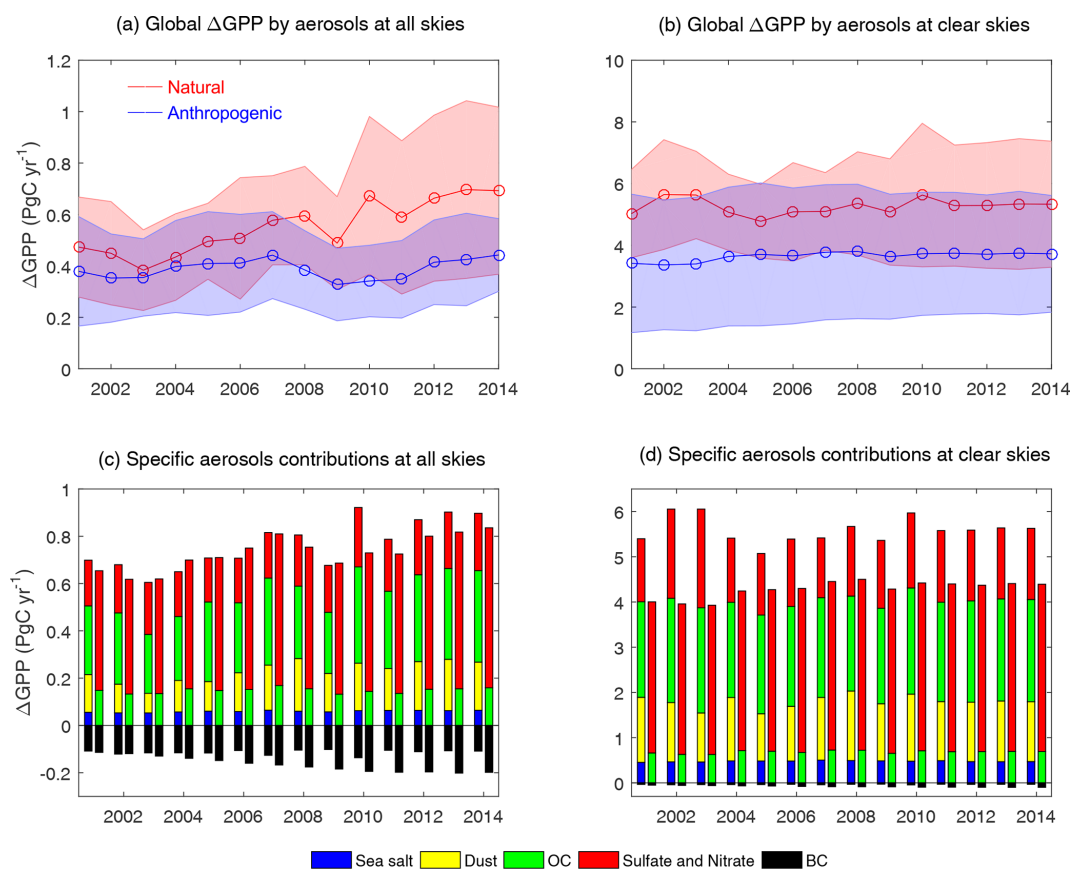


Figure 7. Interannual variations in GPP changes induced by the DFE of natural and anthropogenic aerosols under (a, c) all skies and (b, d) clear skies from 2001–2014. The left and right bars at each year in (c) and (d) represent the effects of natural and anthropogenic aerosol species, respectively. The hollow circles and shadings in (a) and (b) represent annual mean and standard deviation of aerosol-induced GPP changes from all months in each year. The black, green, red, yellow, and blue bars indicate the effects of BC, OC, sulfate and nitrate, dust, and sea salt aerosols, respectively.

diffuse radiation. Observations have shown an optimal diffuse fraction of 0.4–0.6 to enhance GPP for most plant types (Zhou et al., 2021c). A further increase in diffuse fraction above the optimal range will dampen GPP due to the reduced photosynthesis of sunlit leaves. Appearance of cloud has provided an environment with a high diffuse fraction in which aerosols may have limited benefits or even negative effects for GPP (Yue and Unger, 2017). Such a relationship also explains why the decreasing trend of global cloud amount contributes to an increased aerosol DFE (Fig. 7a).

Anthropogenic aerosols account for $\sim 25\%$ of the total aerosol-induced enhancement of diffuse radiation (Fig. 2), while they contribute 41% to the total aerosol DFE under both all- and clear-sky conditions (Fig. 3). The higher efficiency of anthropogenic aerosols in increasing GPP is partly associated with their geographic distribution. Regionally, anthropogenic aerosols take a leading role in DFE over North America, Europe, India, and eastern China, consistent with the estimations by Strada and Unger (2016). On the other hand, natural aerosols dominate DFE in the tropical regions.

Observations have revealed a higher optimal diffuse fraction at higher latitudes, where the higher solar zenith angle induces a larger fraction of shading leaves (Zhou et al., 2021c). As a result, the same amount of diffuse radiation increased by anthropogenic aerosols results in higher GPP enhancement at the middle latitudes than natural aerosols at low latitudes. Furthermore, a dominant fraction of natural aerosols is contributed by dust and sea salt, which increase diffuse radiation over the barren land or open ocean with little forest coverage (Fig. 2). In contrast, most anthropogenic aerosols are located in populous regions covered with dense vegetation. Consequently, the diffuse radiation by anthropogenic aerosols has more interactions with ecosystems than that from natural sources.

Different aerosol species induce varied DFEs to global GPP. Sulfate and nitrate dominate the aerosol-induced GPP changes (Fig. 6) because their strong scattering effects (Gu et al., 2003) largely increase diffuse radiation (Figs. 5 and S7). Keppel-Aleks and Washenfelder (2016) estimated that the regional reductions of sulfate aerosols decreased diffuse

radiation by $0.6\% \text{ yr}^{-1}$ and GPP by $0.07\% \text{ yr}^{-1}$ in the eastern US from 1995–2013. Such negative trends of GPP can also be found over the same region in our clear-sky simulations (Fig. S9b). However, the global ΔGPP shows limited trends under clear-sky conditions (Fig. 7b) because the enhanced SO_2 emissions in China at the same period (Hoesly et al., 2018) increased sulfate loading, promoted local GPP (Fig. S9b), and offset the negative ΔGPP in the eastern US. In our simulations, OC aerosols promote global GPP by $0.47 \text{ Pg C yr}^{-1}$. Such magnitude is much lower than the estimates of $0.76\text{--}1.61 \text{ Pg C yr}^{-1}$ for the same aerosol species by Rap et al. (2018). The main cause of such a discrepancy is related to the predicted aerosol concentrations and radiative effects in two studies (Zhou et al., 2021b). Dust and sea salt aerosols increase regional GPP over arid and coastal regions due to the large local emissions (Yue et al., 2010; Yue and Liao, 2012). Under all-sky conditions, dust exerts a large DFE over North Africa and the Middle East (Fig. 3a) because of the low cloud coverage (Fig. S10). However, such a high GPP ratio shows limited contributions (Fig. 4) to global total ΔGPP because of the extremely low baseline GPP in arid regions. Different from the above species, BC exerts negative impacts on direct and diffuse PAR owing to strong absorbing properties (Kvalevåg and Myhre, 2007). As a result, BC aerosols always decrease GPP with stronger dampening effects under all-sky conditions (Fig. 6c and d) when the light availability is much smaller than that under clear-sky conditions.

4.2 Uncertainties

Our simulations are subject to limitations and uncertainties. First, biases in aerosol profiles may influence the derived aerosol DFE. We used the chemical transport model GEOS-Chem to predict aerosol concentrations and identify contributions from natural and anthropogenic sources. Evaluations showed that GEOS-Chem underestimated global AOD by 25.8%, especially over the Amazon, central Africa, and boreal Asia (Fig. S1) where natural aerosols dominate. In contrast, simulated AOD is overestimated in eastern China where anthropogenic sources dominate. To explore the effects of such underestimation on global aerosol DFE, we performed three additional simulations with 1.5, 2, and 3 times the original aerosol concentrations. Predicted aerosol DFE in these three simulations is respectively 1.13, 1.18, and $0.97 \text{ Pg C yr}^{-1}$ (Fig. S12), similar to the estimate of $0.95 \text{ Pg C yr}^{-1}$ (Fig. 3a) with the original aerosol concentrations. Regionally, aerosols reduce GPP up to -3% over the Amazon, central Africa, India, eastern China, and Indonesia under double or tripled aerosol conditions, which are related to negative effects from high cloud amount (Fig. S11) or aerosol loading (Fig. S1).

Second, the uncertainties of emission inventories may influence the conclusions. In this study, the CEDS emission inventory is used for anthropogenic emissions. Here, we

used another emission database (EDGAR) to assess the uncertainties of DFE from anthropogenic aerosols. The new simulations showed that anthropogenic aerosols increased global GPP by $0.31 \text{ Pg C yr}^{-1}$ (Figs. S13–S14), lower than the value of $0.39 \text{ Pg C yr}^{-1}$ predicted with the CEDS inventory (Fig. 3). The spatial pattern of the percentage contributions remains similar for the two inventories, both of which show dominant impacts by anthropogenic aerosols over eastern China, India, Europe, and North America. For DFE of aerosol species, anthropogenic sulfate and nitrate aerosols still dominate global aerosol DFE up to 28.2%, and natural OC aerosols contribute 18.2% to aerosol DFE (Fig. S15), which is similar to that from CEDS.

Third, uncertainties in the radiative transfer may cause biases to aerosol DFE. Although the CRM was fully validated with observations (Figs. S2 and S3), simulated aerosol radiative effects showed large differences compared to other studies. For example, Chen and Zhuang (2014) found that aerosols increased surface diffuse PAR by 5.2 W m^{-2} using another radiative transfer model. In our simulations, we estimated that aerosols increased diffuse PAR by only 1.26 W m^{-2} . As a result, the GPP enhancement by aerosol DFE is $0.95 \pm 0.13 \text{ Pg C yr}^{-1}$ in our study, much lower than the value of 4.9 Pg C yr^{-1} in Chen and Zhuang (2014), though the latter study also considered aerosol-induced changes in temperature and soil moisture. However, the aerosol radiative effects are likely overestimated in Chen and Zhuang (2014), which predicted total (direct + diffuse) reductions of 21.9 W m^{-2} in surface solar radiation by aerosols; such magnitude is much higher than the multi-model ensemble estimate of -6.3 W m^{-2} under clear-sky conditions (Yu et al., 2006). As a comparison, our simulations showed a reduction of 5.8 W m^{-2} in surface shortwave radiation, much closer to the ensemble estimates by Yu et al. (2006).

Fourth, we ignored the interactive effects among different aerosol species. Although we isolated the impacts of individual aerosol species on global GPP, their non-linear influences still exist in our simulations. For the radiative responses to aerosol species, we found that total aerosols enhance diffuse PAR by 1.26 W m^{-2} (Fig. 2) and reduce direct PAR by 2.78 W m^{-2} (Fig. S4). However, the sum of individual aerosol effects causes a net enhancement of 1.35 W m^{-2} in diffuse PAR (Fig. S5) and a reduction of 2.9 W m^{-2} in direct PAR (Fig. S6), both of which are slightly higher than the effects of all aerosols. Similarly, aerosols enhance global GPP by $0.95 \text{ Pg C yr}^{-1}$ (Fig. 3) but the sum of individual aerosol species enhances global GPP by $1.21 \text{ Pg C yr}^{-1}$ (Fig. 5). Such non-linearity is caused by the complicated responses of individual aerosol species, which can offset each other when they are put together. To facilitate the comparisons, we explore both the absolute (Fig. 6c and d) and actual (Fig. 6e and f) contributions of individual aerosol species to global GPP.

Finally, we neglected the climatic responses to aerosol radiative effects. Surface temperature and relative humidity are altered in response to radiative changes caused by aerosols (Jing et al., 2010; Cirino et al., 2014). The increase in relative humidity can increase plant photosynthesis owing to the enhancement of water use efficiency (Lu et al., 2017; Wang et al., 2021), but the impacts of cooling on photosynthesis are dependent on whether local background temperature is over the optimal temperature (Farquhar et al., 1980). In our previous studies, we explored the direct aerosol radiative effects on NPP in China through changes in radiation, temperature, and soil moisture, and we found that aerosol DFE enhances regional NPP by $0.09 \text{ Pg C yr}^{-1}$, which accounts for $\sim 50\%$ of the total aerosol effects (Yue et al., 2017b). Similarly, Zhang et al. (2021) explored the impacts of anthropogenic aerosols on global carbon sink from 1850–2014 and found that aerosol DFE accounts for 78% of the total aerosol effects on carbon uptake, which is much higher than the effects caused by temperature and precipitation changes. Moreover, the changes in clouds from aerosol indirect effects were not considered in this study. Clouds can significantly influence aerosol DFE because of its strong scattering effects (Fig. 3). The perturbations in clouds can further influence surface temperature, precipitation, and radiation (Zhu et al., 2019), leading to more complex impacts on terrestrial ecosystem productivity. However, these interactive effects by aerosols need to be resolved using Earth system models that implement fully coupled atmospheric chemistry, radiation, land biosphere, and climate feedbacks.

4.3 Implications

Our study reveals that aerosol DFE can enhance global GPP by $0.95 \text{ Pg C yr}^{-1}$ under all-sky conditions and as much as $8.91 \text{ Pg C yr}^{-1}$ under clear-sky conditions. The natural and anthropogenic aerosols make comparable contributions globally but with distinct spatial patterns. The DFE, as well as the climatic effects, suggests that aerosols play important roles in mitigating global warming through direct (cooling) and indirect (more carbon assimilation) processes. Although the reductions of aerosols may weaken the DFE, the associated reductions of cloud amount due to reduced aerosol–cloud interactions may induce more benefits to ecosystems. Furthermore, reductions of black carbon aerosols help relieve both climate warming and GPP inhibitions. Our results suggest that aerosol DFE should be considered in projecting future changes in terrestrial ecosystem productivity, especially for different emission scenarios.

Data availability. The simulated GPP and diffuse PAR caused by natural and anthropogenic aerosols in this paper are publicly available via Zenodo (<https://doi.org/10.5281/zenodo.5115314>; Zhou and Yue, 2021).

Supplement. The supplement related to this article is available online at: <https://doi.org/10.5194/acp-22-693-2022-supplement>.

Author contributions. XuY conceived the study. XuY, HZ, and YL designed the research and performed simulations. HZ completed data analysis and the first draft. XuY reviewed and edited the manuscript. CT, JZ, YM, YC, XiY, and ZZ were responsible for data collection processes.

Competing interests. The contact author has declared that neither they nor their co-authors have any competing interests.

Disclaimer. Publisher's note: Copernicus Publications remains neutral with regard to jurisdictional claims in published maps and institutional affiliations.

Acknowledgements. The authors thank the reviewers for their constructive comments and thoughtful suggestions, and all data or model codes used in this study are available via websites in the Methods section.

Financial support. This research has been supported by the National Key Research and Development Program of China (grant no. 2019YFA0606802) and Jiangsu Science Fund for Distinguished Young Scholars (grant no. BK20200040).

Review statement. This paper was edited by Dominick Spracklen and reviewed by two anonymous referees.

References

- Alton, P. B.: Reduced carbon sequestration in terrestrial ecosystems under overcast skies compared to clear skies, *Agric. Forest Meteorol.*, 148, 1641–1653, <https://doi.org/10.1016/j.agrformet.2008.05.014>, 2008.
- Alton, P. B., North, P. R., and Los, S. O.: The impact of diffuse sunlight on canopy light-use efficiency, gross photosynthetic product and net ecosystem exchange in three forest biomes, *Global Change Biol.*, 13, 776–787, <https://doi.org/10.1111/j.1365-2486.2007.01316.x>, 2007.
- Ball, J. T., Woodrow, I. E., and Berry, J. A.: A Model Predicting Stomatal Conductance and its Contribution to the Control of Photosynthesis under Different Environmental Conditions, in: *Progress in Photosynthesis Research: Volume 4 Proceedings of the VIIth International Congress on Photosynthesis Providence, Rhode Island, USA, 10–15 August 1986*, edited by: Biggins, J., Springer Netherlands, Dordrecht, 221–224, 1987.
- Bey, I., Jacob, D. J., Yantosca, R. M., Logan, J. A., Field, B. D., Fiore, A. M., Li, Q. B., Liu, H. G. Y., Mickley, L. J., and Schultz, M. G.: Global modeling of tropospheric chemistry with assimilated meteorology: Model description

- and evaluation, *J. Geophys. Res.-Atmos.*, 106, 23073–23095, <https://doi.org/10.1029/2001jd000807>, 2001.
- Breider, T. J., Mickley, L. J., Jacob, D. J., Ge, C., Wang, J., Payer Sulprizio, M., Croft, B., Ridley, D. A., McConnell, J. R., Sharma, S., Husain, L., Dutkiewicz, V. A., Eleftheriadis, K., Skov, H., and Hopke, P. K.: Multidecadal trends in aerosol radiative forcing over the Arctic: Contribution of changes in anthropogenic aerosol to Arctic warming since 1980, *J. Geophys. Res.-Atmos.*, 122, 3573–3594, <https://doi.org/10.1002/2016JD025321>, 2017.
- Chen, M. and Zhuang, Q.: Evaluating aerosol direct radiative effects on global terrestrial ecosystem carbon dynamics from 2003 to 2010, *Tellus B*, 66, 21808, <https://doi.org/10.3402/tellusb.v66.21808>, 2014.
- Cirino, G. G., Souza, R. A. F., Adams, D. K., and Artaxo, P.: The effect of atmospheric aerosol particles and clouds on net ecosystem exchange in the Amazon, *Atmos. Chem. Phys.*, 14, 6523–6543, <https://doi.org/10.5194/acp-14-6523-2014>, 2014.
- Cohan, D. S., Xu, J., Greenwald, R., Bergin, M. H., and Chameides, W. L.: Impact of atmospheric aerosol light scattering and absorption on terrestrial net primary productivity, *Global Biogeochem. Cycles*, 16, 1090, <https://doi.org/10.1029/2001gb001441>, 2002.
- Doughty, C. E., Flanner, M. G., and Goulden, M. L.: Effect of smoke on subcanopy shaded light, canopy temperature, and carbon dioxide uptake in an Amazon rainforest, *Global Biogeochem. Cycles*, 24, GB3015, <https://doi.org/10.1029/2009gb003670>, 2010.
- Ezhova, E., Ylivinkka, I., Kuusk, J., Komsaare, K., Vana, M., Krasnova, A., Noe, S., Arshinov, M., Belan, B., Park, S.-B., Lavrič, J. V., Heimann, M., Petäjä, T., Vesala, T., Mammarella, I., Kolari, P., Bäck, J., Rannik, Ü., Kerminen, V.-M., and Kulmala, M.: Direct effect of aerosols on solar radiation and gross primary production in boreal and hemiboreal forests, *Atmos. Chem. Phys.*, 18, 17863–17881, <https://doi.org/10.5194/acp-18-17863-2018>, 2018.
- Farquhar, G. D., Caemmerer, S. V., and Berry, J. A.: A biochemical-model of photosynthetic CO₂ assimilation in leaves of C-3 species, *Planta*, 149, 78–90, <https://doi.org/10.1007/bf00386231>, 1980.
- Fisher, J. A., Jacob, D. J., Wang, Q., Bahreini, R., Carouge, C. C., Cubison, M. J., Dibb, J. E., Diehl, T., Jimenez, J. L., Leibensperger, E. M., Lu, Z., Meinders, M. B. J., Pye, H. O. T., Quinn, P. K., Sharma, S., Streets, D. G., van Donkelaar, A., and Yantosca, R. M.: Sources, distribution, and acidity of sulfate–ammonium aerosol in the Arctic in winter–spring, *Atmos. Environ.*, 45, 7301–7318, <https://doi.org/10.1016/j.atmosenv.2011.08.030>, 2011.
- Friedlingstein, P., O’Sullivan, M., Jones, M. W., Andrew, R. M., Hauck, J., Olsen, A., Peters, G. P., Peters, W., Pongratz, J., Sitch, S., Le Quééré, C., Canadell, J. G., Ciais, P., Jackson, R. B., Alin, S., Aragão, L. E. O. C., Armeth, A., Arora, V., Bates, N. R., Becker, M., Benoit-Cattin, A., Bittig, H. C., Bopp, L., Bultan, S., Chandra, N., Chevallier, F., Chini, L. P., Evans, W., Florentie, L., Forster, P. M., Gasser, T., Gehlen, M., Gilfillan, D., Gkritzalis, T., Gregor, L., Gruber, N., Harris, I., Hartung, K., Haverd, V., Houghton, R. A., Ilyina, T., Jain, A. K., Joetzjer, E., Kadono, K., Kato, E., Kitidis, V., Korsbakken, J. I., Landschützer, P., Lefèvre, N., Lenton, A., Lienert, S., Liu, Z., Lombardozzi, D., Marland, G., Metzl, N., Munro, D. R., Nabel, J. E. M. S., Nakaoka, S.-I., Niwa, Y., O’Brien, K., Ono, T., Palmer, P. I., Pierrot, D., Poulter, B., Resplandy, L., Robertson, E., Rödenbeck, C., Schwinger, J., Séférian, R., Skjelvan, I., Smith, A. J. P., Sutton, A. J., Tans, P. P., Tian, H., Tilbrook, B., van der Werf, G., Vuichard, N., Walker, A. P., Wanninkhof, R., Watson, A. J., Willis, D., Wiltshire, A. J., Yuan, W., Yue, X., and Zaehle, S.: Global Carbon Budget 2020, *Earth Syst. Sci. Data*, 12, 3269–3340, <https://doi.org/10.5194/essd-12-3269-2020>, 2020.
- Giorgi, F., Coppola, E., Solmon, F., Mariotti, L., Sylla, M. B., Bi, X., Elguindi, N., Diro, G. T., Nair, V., Giuliani, G., Turuncoglu, U. U., Cozzini, S., Guttler, I., O’Brien, T. A., Tawfik, A. B., Shalaby, A., Zakey, A. S., Steiner, A. L., Stordal, F., Sloan, L. C., and Brankovic, C.: RegCM4: model description and preliminary tests over multiple CORDEX domains, *Climate Res.*, 52, 7–29, <https://doi.org/10.3354/cr01018>, 2012.
- Gu, L. H., Baldocchi, D., Verma, S. B., Black, T. A., Vesala, T., Falge, E. M., and Dowty, P. R.: Advantages of diffuse radiation for terrestrial ecosystem productivity, *J. Geophys. Res.-Atmos.*, 107, 4050, <https://doi.org/10.1029/2001jd001242>, 2002.
- Gu, L. H., Baldocchi, D. D., Wofsy, S. C., Munger, J. W., Michalsky, J. J., Urbanski, S. P., and Boden, T. A.: Response of a deciduous forest to the Mount Pinatubo eruption: Enhanced photosynthesis, *Science*, 299, 2035–2038, <https://doi.org/10.1126/science.1078366>, 2003.
- Guenther, A. B., Jiang, X., Heald, C. L., Sakulyanontvittaya, T., Duhl, T., Emmons, L. K., and Wang, X.: The Model of Emissions of Gases and Aerosols from Nature version 2.1 (MEGAN2.1): an extended and updated framework for modeling biogenic emissions, *Geosci. Model Dev.*, 5, 1471–1492, <https://doi.org/10.5194/gmd-5-1471-2012>, 2012.
- He, M. Z., Ju, W. M., Zhou, Y. L., Chen, J. M., He, H. L., Wang, S. Q., Wang, H. M., Guan, D. X., Yan, J. H., Li, Y. N., Hao, Y. B., and Zhao, F. H.: Development of a two-leaf light use efficiency model for improving the calculation of terrestrial gross primary productivity, *Agric. Forest Meteorol.*, 173, 28–39, <https://doi.org/10.1016/j.agrformet.2013.01.003>, 2013.
- Hemes, K. S., Verfaillie, J., and Baldocchi, D. D.: Wildfire-Smoke Aerosols Lead to Increased Light Use Efficiency Among Agricultural and Restored Wetland Land Uses in California’s Central Valley, *J. Geophys. Res.-Biogeo.*, 125, 21, <https://doi.org/10.1029/2019jg005380>, 2020.
- Hoesly, R. M., Smith, S. J., Feng, L., Klimont, Z., Janssens-Maenhout, G., Pitkanen, T., Seibert, J. J., Vu, L., Andres, R. J., Bolt, R. M., Bond, T. C., Dawidowski, L., Kholod, N., Kurokawa, J.-I., Li, M., Liu, L., Lu, Z., Moura, M. C. P., O’Rourke, P. R., and Zhang, Q.: Historical (1750–2014) anthropogenic emissions of reactive gases and aerosols from the Community Emissions Data System (CEDS), *Geosci. Model Dev.*, 11, 369–408, <https://doi.org/10.5194/gmd-11-369-2018>, 2018.
- Jaeglé, L., Quinn, P. K., Bates, T. S., Alexander, B., and Lin, J.-T.: Global distribution of sea salt aerosols: new constraints from in situ and remote sensing observations, *Atmos. Chem. Phys.*, 11, 3137–3157, <https://doi.org/10.5194/acp-11-3137-2011>, 2011.
- Jing, X., Huang, J., Wang, G., Higuchi, K., Bi, J., Sun, Y., Yu, H., and Wang, T.: The effects of clouds and aerosols on net ecosystem CO₂ exchange over semi-arid Loess Plateau of Northwest China, *Atmos. Chem. Phys.*, 10, 8205–8218, <https://doi.org/10.5194/acp-10-8205-2010>, 2010.
- Kanniah, K. D., Beringer, J., and Hurley, L.: Exploring the link between clouds, radiation, and canopy productivity of

- tropical savannas, *Agric. Forest Meteorol.*, 182, 304–313, <https://doi.org/10.1016/j.agrformet.2013.06.010>, 2013.
- Keppel-Aleks, G. and Washenfelder, R. A.: The effect of atmospheric sulfate reductions on diffuse radiation and photosynthesis in the United States during 1995–2013, *Geophys. Res. Lett.*, 43, 9984–9993, <https://doi.org/10.1002/2016gl070052>, 2016.
- Kinne, S.: Aerosol radiative effects with MACv2, *Atmos. Chem. Phys.*, 19, 10919–10959, <https://doi.org/10.5194/acp-19-10919-2019>, 2019.
- Kvalevåg, M. M. and Myhre, G.: Human Impact on Direct and Diffuse Solar Radiation during the Industrial Era, *J. Climate*, 20, 4874–4883, <https://doi.org/10.1175/jcli4277.1>, 2007.
- Li, X. and Xiao, J.: Mapping Photosynthesis Solely from Solar-Induced Chlorophyll Fluorescence: A Global, Fine-Resolution Dataset of Gross Primary Production Derived from OCO-2, *Remote Sens.*, 11, 2563, <https://doi.org/10.3390/rs11212563>, 2019.
- Lu, X., Chen, M., Liu, Y., Miralles, D. G., and Wang, F.: Enhanced water use efficiency in global terrestrial ecosystems under increasing aerosol loadings, *Agric. Forest Meteorol.*, 237, 39–49, <https://doi.org/10.1016/j.agrformet.2017.02.002>, 2017.
- Malavelle, F. F., Haywood, J. M., Mercado, L. M., Folberth, G. A., Bellouin, N., Sitch, S., and Artaxo, P.: Studying the impact of biomass burning aerosol radiative and climate effects on the Amazon rainforest productivity with an Earth system model, *Atmos. Chem. Phys.*, 19, 1301–1326, <https://doi.org/10.5194/acp-19-1301-2019>, 2019.
- Matsui, T., Beltran-Przekurat, A., Niyogi, D., Pielke, R. A., Sr., and Coughenour, M.: Aerosol light scattering effect on terrestrial plant productivity and energy fluxes over the eastern United States, *J. Geophys. Res.-Atmos.*, 113, D14S14, <https://doi.org/10.1029/2007jd009658>, 2008.
- Mercado, L. M., Bellouin, N., Sitch, S., Boucher, O., Huntingford, C., Wild, M., and Cox, P. M.: Impact of changes in diffuse radiation on the global land carbon sink, *Nature*, 458, 1014–1087, <https://doi.org/10.1038/nature07949>, 2009.
- Moreira, D. S., Longo, K. M., Freitas, S. R., Yamasoe, M. A., Mercado, L. M., Rosário, N. E., Gloor, E., Viana, R. S. M., Miller, J. B., Gatti, L. V., Wiedemann, K. T., Domingues, L. K. G., and Correia, C. C. S.: Modeling the radiative effects of biomass burning aerosols on carbon fluxes in the Amazon region, *Atmos. Chem. Phys.*, 17, 14785–14810, <https://doi.org/10.5194/acp-17-14785-2017>, 2017.
- Nascimento, J. P., Bela, M. M., Meller, B. B., Banducci, A. L., Rizzo, L. V., Vara-Vela, A. L., Barbosa, H. M. J., Gomes, H., Rafee, S. A. A., Franco, M. A., Carbone, S., Cirino, G. G., Souza, R. A. F., McKeen, S. A., and Artaxo, P.: Aerosols from anthropogenic and biogenic sources and their interactions – modeling aerosol formation, optical properties, and impacts over the central Amazon basin, *Atmos. Chem. Phys.*, 21, 6755–6779, <https://doi.org/10.5194/acp-21-6755-2021>, 2021.
- Paulot, F., Paynter, D., Ginoux, P., Naik, V., and Horowitz, L. W.: Changes in the aerosol direct radiative forcing from 2001 to 2015: observational constraints and regional mechanisms, *Atmos. Chem. Phys.*, 18, 13265–13281, <https://doi.org/10.5194/acp-18-13265-2018>, 2018.
- Rap, A., Spracklen, D. V., Mercado, L., Reddington, C. L., Haywood, J. M., Ellis, R. J., Phillips, O. L., Artaxo, P., Bonal, D., Coupe, N. R., and Butt, N.: Fires increase Amazon forest productivity through increases in diffuse radiation, *Geophys. Res. Lett.*, 42, 4654–4662, <https://doi.org/10.1002/2015gl063719>, 2015.
- Rap, A., Scott, C. E., Reddington, C. L., Mercado, L., Ellis, R. J., Garraway, S., Evans, M. J., Beerling, D. J., MacKenzie, A. R., Hewitt, C. N., and Spracklen, D. V.: Enhanced global primary production by biogenic aerosol via diffuse radiation fertilization, *Nat. Geosci.*, 11, 640, <https://doi.org/10.1038/s41561-018-0208-3>, 2018.
- Roderick, M. L., Farquhar, G. D., Berry, S. L., and Noble, I. R.: On the direct effect of clouds and atmospheric particles on the productivity and structure of vegetation, *Oecologia*, 129, 21–30, <https://doi.org/10.1007/s004420100760>, 2001.
- Ryu, Y.-H., Baik, J.-J., and Lee, S.-H.: Effects of anthropogenic heat on ozone air quality in a megacity, *Atmos. Environ.*, 80, 20–30, <https://doi.org/10.1016/j.atmosenv.2013.07.053>, 2013.
- Spitters, C. J. T., Toussaint, H., and Goudriaan, J.: Separating the diffuse and direct component of global radiation and its implications for modeling canopy photosynthesis Part 1. components of incoming radiation, *Agric. Forest Meteorol.*, 38, 217–229, [https://doi.org/10.1016/0168-1923\(86\)90060-2](https://doi.org/10.1016/0168-1923(86)90060-2), 1986.
- Strada, S. and Unger, N.: Potential sensitivity of photosynthesis and isoprene emission to direct radiative effects of atmospheric aerosol pollution, *Atmos. Chem. Phys.*, 16, 4213–4234, <https://doi.org/10.5194/acp-16-4213-2016>, 2016.
- Strada, S., Unger, N., and Yue, X.: Observed aerosol-induced radiative effect on plant productivity in the eastern United States, *Atmos. Environ.*, 122, 463–476, <https://doi.org/10.1016/j.atmosenv.2015.09.051>, 2015.
- Wang, B., Wang, Z., Wang, C., Wang, X., Li, J., Jia, Z., Li, P., Wu, J., Chen, M., and Liu, L.: Field evidence reveals conservative water use of poplar saplings under high aerosol conditions, *J. Ecol.*, 109, 2190–2202, <https://doi.org/10.1111/1365-2745.13633>, 2021.
- Wang, X., Wu, J., Chen, M., Xu, X., Wang, Z., Wang, B., Wang, C., Piao, S., Lin, W., Miao, G., Deng, M., Qiao, C., Wang, J., Xu, S., and Liu, L.: Field evidences for the positive effects of aerosols on tree growth, *Global Change Biol.*, 24, 4983–4992, <https://doi.org/10.1111/gcb.14339>, 2018.
- Xie, X., Wang, T., Yue, X., Li, S., Zhuang, B., and Wang, M.: Effects of atmospheric aerosols on terrestrial carbon fluxes and CO₂ concentrations in China, *Atmos. Res.*, 237, 104859, <https://doi.org/10.1016/j.atmosres.2020.104859>, 2020.
- Yu, H., Kaufman, Y. J., Chin, M., Feingold, G., Remer, L. A., Anderson, T. L., Balkanski, Y., Bellouin, N., Boucher, O., Christopher, S., DeCola, P., Kahn, R., Koch, D., Loeb, N., Reddy, M. S., Schulz, M., Takemura, T., and Zhou, M.: A review of measurement-based assessments of the aerosol direct radiative effect and forcing, *Atmos. Chem. Phys.*, 6, 613–666, <https://doi.org/10.5194/acp-6-613-2006>, 2006.
- Yue, X. and Liao, H.: Climatic responses to the shortwave and long-wave direct radiative effects of sea salt aerosol in present day and the last glacial maximum, *Clim. Dynam.*, 39, 3019–3040, <https://doi.org/10.1007/s00382-012-1312-5>, 2012.
- Yue, X. and Unger, N.: The Yale Interactive terrestrial Biosphere model version 1.0: description, evaluation and implementation into NASA GISS ModelE2, *Geosci. Model Dev.*, 8, 2399–2417, <https://doi.org/10.5194/gmd-8-2399-2015>, 2015.
- Yue, X. and Unger, N.: Aerosol optical depth thresholds as a tool to assess diffuse radiation fertilization of the land car-

- bon uptake in China, *Atmos. Chem. Phys.*, 17, 1329–1342, <https://doi.org/10.5194/acp-17-1329-2017>, 2017.
- Yue, X. and Unger, N.: Fire air pollution reduces global terrestrial productivity, *Nat. Commun.*, 9, 5413, <https://doi.org/10.1038/s41467-018-07921-4>, 2018.
- Yue, X., Wang, H. J., Liao, H., and Fan, K.: Simulation of dust aerosol radiative feedback using the GMOD: 2. Dust-climate interactions, *J. Geophys. Res.-Atmos.*, 115, D04201, <https://doi.org/10.1029/2009jd012063>, 2010.
- Yue, X., Unger, N., and Zheng, Y.: Distinguishing the drivers of trends in land carbon fluxes and plant volatile emissions over the past 3 decades, *Atmos. Chem. Phys.*, 15, 11931–11948, <https://doi.org/10.5194/acp-15-11931-2015>, 2015.
- Yue, X., Strada, S., Unger, N., and Wang, A.: Future inhibition of ecosystem productivity by increasing wildfire pollution over boreal North America, *Atmos. Chem. Phys.*, 17, 13699–13719, <https://doi.org/10.5194/acp-17-13699-2017>, 2017a.
- Yue, X., Unger, N., Harper, K., Xia, X., Liao, H., Zhu, T., Xiao, J., Feng, Z., and Li, J.: Ozone and haze pollution weakens net primary productivity in China, *Atmos. Chem. Phys.*, 17, 6073–6089, <https://doi.org/10.5194/acp-17-6073-2017>, 2017b.
- Yue, X., Zhang, T., and Shao, C.: Afforestation increases ecosystem productivity and carbon storage in China during the 2000s, *Agric. Forest Meteorol.*, 296, 108227, <https://doi.org/10.1016/j.agrformet.2020.108227>, 2021.
- Zhang, Y., Ciais, P., Boucher, O., Maignan, F., Bastos, A., Goll, D., Lurton, T., Viovy, N., Bellouin, N., and Li, L.: Disentangling the Impacts of Anthropogenic Aerosols on Terrestrial Carbon Cycle During 1850–2014, *Earth's Future*, 9, e2021EF002035, <https://doi.org/10.1029/2021EF002035>, 2021.
- Zhou, H. and Yue, X.: Data for Aerosol Diffuse Fertilization Effect (Version V1), Zenodo [data set], <https://doi.org/10.5281/zenodo.5115314>, 2021.
- Zhou, H., Yue, X., Lei, Y., Tian, C., Ma, Y., and Cao, Y.: Large Contributions of Diffuse Radiation to Global Gross Primary Productivity During 1981–2015, *Global Biogeochem. Cycles*, 35, e2021GB006957, <https://doi.org/10.1029/2021GB006957>, 2021a.
- Zhou, H., Yue, X., Lei, Y., Tian, C., Ma, Y., and Cao, Y.: Aerosol radiative and climatic effects on ecosystem productivity and evapotranspiration, *Curr. Opin. Environ. Sci. He.*, 19, 100218, <https://doi.org/10.1016/j.coesh.2020.10.006>, 2021b.
- Zhou, H., Yue, X., Lei, Y., Zhang, T., Tian, C., Ma, Y., and Cao, Y.: Responses of gross primary productivity to diffuse radiation at global FLUXNET sites, *Atmos. Environ.*, 244, 117905, <https://doi.org/10.1016/j.atmosenv.2020.117905>, 2021c.
- Zhu, P. Y., Cheng, S. J., Butterfield, Z., Keppel-Aleks, G., and Steiner, A. L.: The Global Influence of Cloud Optical Thickness on Terrestrial Carbon Uptake, *Earth Interact.*, 23, 22, <https://doi.org/10.1175/ei-d-17-0035.1>, 2019.